Opto-mechanical analyses for performance optimization of lightweight grazing-incidence mirrors

Jacqueline M. Roche, Jeffery J. Kolodziejczak, Stephen L. O'Dell, Ronald F. Elsner, Martin C. Weisskopf, Brian Ramsey, and Mikhail V. Gubarev

NASA Marshall Space Flight Center, Space Science Office, MSFC/ZP12, Huntsville, AL 35812

ABSTRACT

New technology in grazing-incidence mirror fabrication and assembly is necessary to achieve sub-arcsecond optics for large-area x-ray telescopes. In order to define specifications, an understanding of performance sensitivity to design parameters is crucial. MSFC is undertaking a systematic study to specify a mounting approach, mirror substrate, and testing method. Lightweight mirrors are typically flimsy and are, therefore, susceptible to significant distortion due to mounting and gravitational forces. Material properties of the mirror substrate along with its dimensions significantly affect the distortions caused by mounting and gravity. A parametric study of these properties and their relationship to mounting and testing schemes will indicate specifications for the design of the next generation of lightweight grazing-incidence mirrors. Here we report initial results of this study.

Keywords: X-ray telescopes, opto-mechanical analysis techniques.

1. INTRODUCTION

More than 14 years have passed since the launch of the *Chandra X-ray Observatory,*[1,2,3] and it maintains its distinction as the first and only mission to attain sub-arcsecond x-ray imaging. The limitation of fabricating its precise 4 massive mirror pairs is that it only has 750 cm^2 of effective area. Conversely, XMM-Newton has 5.5-times larger effective area but is limited by less precise shells that result in ~30 times the half-energy width of *Chandra*.[4,5,6] The purpose of new technology is to get rid of limitations from the past. We cannot fit more robust, *Chandra*-like shells into the available volume and mass constraints, so we must construct and assemble thinner and/or lighter, high-resolution mirrors. Development efforts toward mirror fabrication have been proceeding for decades and now appear to be approaching success. In anticipation, we are beginning to prepare for the technical challenges associated with assembling and supporting lightweight, sub-arcsecond mirrors without degrading their performance.

In this paper we first survey the status of technologies associated with x-ray mirror fabrication, mounting and assembly, then discuss our plans for addressing issues associated with constructing densely packed, high-precision grazing-incidence mirror modules. Finally, we will describe our initial progress in understanding the opto-mechanics of the problem for a specific simple configuration.

1.1. Current state of x-ray optics mounting and assembly technology

Most current designs for x-ray telescopes employ grazing-incidence (Wolter-1-like) mirror pairs, as does *Chandra,* but add more light-weight shells to the nested design.[7] The full-shell x-ray optics are typically fabricated using replication off a precision mandrel in order to enable both precision and thin shells.[8] Another potential fabrication method for the thin, full-cylindrical shells is direct fabrication using low-stress polishing.[9] Slumped glass and silicon pore optics are options for segmented x-ray optics.[10] Differential deposition[11] and active figure control[12] are both valid possibilities in improving the performance of thin x-ray optics.

A lot of the current mounts for x-ray optics are fixed, however passive flexures have been used in various designs including Chandra. Active mount figure control is also being investigated.

2. APPROACH

There are many approaches, each with many parameters, for producing lightweight grazing-incidence mirror modules. In this section we outline the philosophical basis for our approach and then describe our plan for developing optimization paths through the myriad possibilities and pitfalls. The principal tools include analytical modeling, finite-element modeling, and metrology.

2.1. Assumptions and philosophy

In order to focus our attention on mounting issues, we assume that we start with a mirror that is perfect in its free state. We also follow four guidelines to avoid being distracted by other complications.

1. Do not design the mirror assembly to address thermal and vibrational considerations. Initially, assume that external hardware will provide adequate thermal stability and vibration isolation.
2. Do not design the mirror assembly for 1-g operations in a horizontal orientation. Assume that the mirror assembly will be vertical during alignment, assembly, metrology, and x-ray testing.
3. Do not design the mirror assembly to satisfy an arbitrary mass limit. Scientific performance should take precedence over initial programmatic constraints on mass, to the extent possible.
4. Make our goal sub-arcsecond imaging. Achieving 5" would indicate progress, but it's not where we need to be.

2.2. Development plan

•Start with simple configurations

The initial configuration is a simple cylindrical shell shown in Figure 1, with attributes matching a cylindrical test article in our laboratory. We use a three-point mount configuration and assume a 10 μm radial distortion at each point, simulating a potential mounting error. The performance analysis for each mounting location was analyzed with two independent models, for points varying axially along the cylinder.

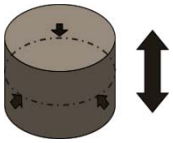

Figure 1: Simple cylindrical configuration used to better understand mounting errors; three-point radial distortions applied.

• **Validate**

The performance analysis of the cylindrical shell was performed, using both analytical methods and finite element analysis (FEA). Analytical methods were applied in Mathematica® and detailed finite element models (FEMs) were made in ANSYS. Eventually, we plan to use metrology to extract experimental data in order to validate the analytical models.

• **Explore parameter space with analytical models**

By using Mathematica® code, we produce low-order expansions of performance solutions and quickly explore a large volume of parameter space. Trends and stark contrasts are more readily identified using this approach.

• **Verify conclusions with FEA**

The models developed in FEA are more detail-oriented and will allow more fine-tuned adjustments. The detailed models will help us to hone in on the specifics of an optimal mounting design.

• **Add required complexity to FEMs, gauging contributions to performance from each**

We are studying the top-level parameters by keeping the models simple. The next stage of analysis will be to add the required complexity. The first parameter we will add is the prescription of the grazing incidence optic and the effect of the primary-secondary interface. We will also consider the effects of bonding under a gravity load as well as the effect of gravity on the shells during metrology. Once we have analyzed all these effects, we will modify some of the details of the mounts and study the impact on performance. Eventually, we will analyze mounting configurations for segmented designs and also determine the impact of using active components.

• **Build and test prototypes**

The final step will be to manufacture a prototype design. Our validation approach is shown in Figure 2.

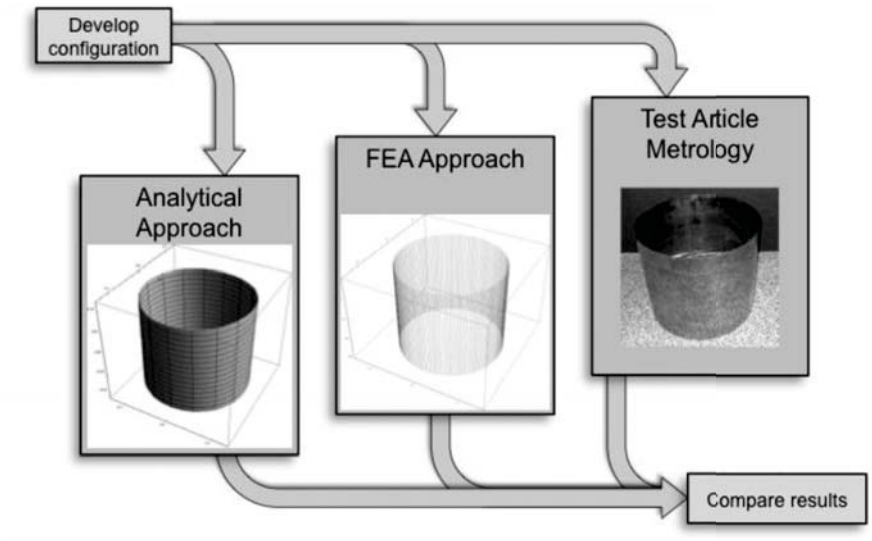

Figure 2: Our validation approach.

2.3.Analytical Modeling

We have started developing analytical modeling capability in Mathematica® as an auxiliary tool for design optimization. These are several benefits:

- ✓ gain insight into performance drivers
- ✓ rapid determination of optimal parameter configurations and of performance sensitivity to each parameter
- ✓ rapid and flexible visualization of mounting effects
- ✓ reduces number of FEMs required to converge on an optimal solution
- ✓ provides a valid comparison for FEA results

The distinction from FEA is primarily in the workflow. In order to do a parametric study in FEA, one must start with a precise design and then vary parameters over a specified range. The processing steps include: generate a model, solve for deflections, generate and store the data, and analyze the data for each parameter for each case. The analytical approach requires less initial knowledge and enables a more flexible and exploratory workflow.

For x-ray optics using small grazing angles, we require computational analysis between each node. Calculations of slope data along with large optical surfaces require a large numbers of nodes. These models are resource-consuming to execute over large multidimensional parametric grids, so it is even more beneficial to focus FEA tools on key regions of parameter space. In addition, our FEA resources are somewhat limited due to the variety of other high-priority tasks currently scheduled.

We have begun our analytical modeling by examining thin cylindrical shells. Kirchoff-Love Theory,[13] describes the linear deflection of thin elastic shells. The theory assumes that strains normal to the shell middle surface can be neglected and that displacements are small compared to the shell thickness (we sometimes ignore this for visualization purposes). Following the plan described in Section 2.2, we begin with a simple configuration, a cylindrical shell, neglecting any effects of cone angles and figure, with a coplanar set of mounting points orthogonal to the optical axis.

The initial model was developed in Mathematica®. The basic steps in the process are these: first select mounting locations and characteristics; next determine boundary conditions; and finally solve for deflections using variational principles for the stationary point of the static total Lagrangian. We expand the mounting load in terms of harmonics of azimuthal angle, θ. The deflection, η, as a function of θ and axial coordinate, z, is governed by the equation:

$$\nabla^2 \nabla^2 \eta(\theta, z) = C\, \delta(z - z1) \sum_{n=0}^{\infty} k(n, 1) \cos(\theta\, n) + k(n, 2) \sin(\theta\, n)$$

We place the coefficient indices in parentheses rather than subscript, and z1 is the axial mounting location. The solution for the for the n^{th} harmonic of θ has the form,

$$f(n, \theta, z, R, z1) =$$
$$\cos(\theta\, n)\left(\frac{a(n,1,5)}{2\,n^3}\,\theta(z-z1)\left(\frac{n\,(z-z1)}{R}\cosh\left(\frac{n\,(z-z1)}{R}\right)-\sinh\left(\frac{n\,(z-z1)}{R}\right)\right)+a(n,1,3)\sinh\left(\frac{n\,z}{R}\right)+a(n,1,4)\,\frac{n\,z}{R}\sinh\left(\frac{n\,z}{R}\right)+a(n,1,1)\cosh\left(\frac{n\,z}{R}\right)+a(n,1,2)\,\frac{n\,z}{R}\cosh\left(\frac{n\,z}{R}\right)\right)+$$
$$\sin(\theta\, n)\left(\frac{a(n,2,5)}{2\,n^3}\,\theta(z-z1)\left(\frac{n\,(z-z1)}{R}\cosh\left(\frac{n\,(z-z1)}{R}\right)-\sinh\left(\frac{n\,(z-z1)}{R}\right)\right)+a(n,2,3)\sinh\left(\frac{n\,z}{R}\right)+a(n,2,4)\,\frac{n\,z}{R}\sinh\left(\frac{n\,z}{R}\right)+a(n,2,1)\cosh\left(\frac{n\,z}{R}\right)+\frac{n\,z}{R}\,a(n,2,2)\cosh\left(\frac{n\,z}{R}\right)\right)$$

Here, R is the shell radius. Initially, we model a 3 point mounting scheme, and only the second and third harmonics are included in the model. We will add higher orders as necessary to validate against the FEA and actual shell measurements.

We also use Mathematica® for visualization as shown in Figure 3, where the mounting points are near the edge of the shell. The left plot depicts the deformed shell in 3 dimensions, the plots on the right show a polar plot of the azimuthal profile in the mounting plane, the axial profile at the 3 mounting meridians, a polar plot of the mean displacement vs. azimuth, and a polar plot of the 2-reflection angular error (see Section 3.3) vs. azimuth. This visualization of parametric sensitivities is very useful. For example, by generating a series of these models with some parameters varied and assembling them into an animation, it is possible to visualize the effect in 4 dimensions.

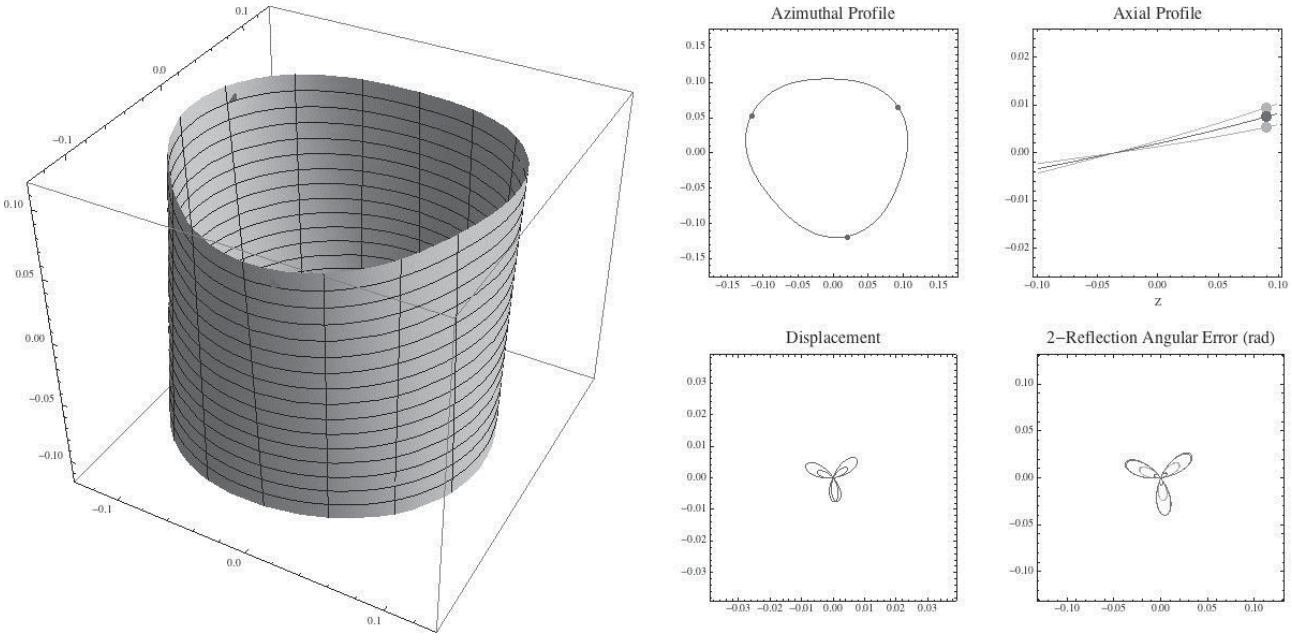

Figure 3: An example of using analytical modeling to gain insight through visualization. A deformed shell is shown on the left. The plots on the right show the azimuthal profile in the mounting plane (points are mounting locations), the axial profile of the mounting meridians, the mean displacement vs. azimuth, and the 2-reflection angular error vs. azimuth. The 2-reflection angular error is discussed in Section 3.3.

2.4. Finite Element Modeling (FEM)

The engineering standard for static structural analysis is FEM. For optical design, developers generally use this modeling tool for normal-incidence optics as a guide to stiffen elements. A parametric study is usually performed to minimize stress on the optic during launch and to minimize distortions due to gravity, mounting forces, thermal gradients and manufacturing errors. The thin

optical elements and the grazing incidence configuration required for lightweight x-ray optics necessitates a new design regime.

The next generation of x-ray optics requires advancements in many areas: vibrational control during launch, thermal control in orbit, rocketry (allowing more weight), and mounting techniques with gravitational load. For the purpose of advancing the optics for x-ray astronomy, we are currently assuming these parameters have no effect on the design, as summarized in Section 2.1.

The goal of our study is to mount thin, precise optics with as little induced distortion as possible. Although the parameter space is very different from a typical opto-mechanical engineering analysis, many of the objectives are the same: minimize mounting distortions due to gravity, minimize metrology error due to gravity, and minimize effect of tolerancing errors.

Because of the design of grazing incidence optics, the change in slope due to optical errors is the determining factor in the optic's performance. A higher precision of output from FEA is necessary, because the raw data must be processed. Calculating the optical error for grazing incidence optics also differs from normal-incidence optics. The wavefront error for normal-incidence optics is one-to-one with the distortion of the optical surface, but the optical performance must be calculated for grazing incidence optics. These calculations necessitate a high mesh density and high precision output from FEA.

On the left in Figure 4 is a FEM of a mirror shell held at the end, with the resulting surface error on the right.

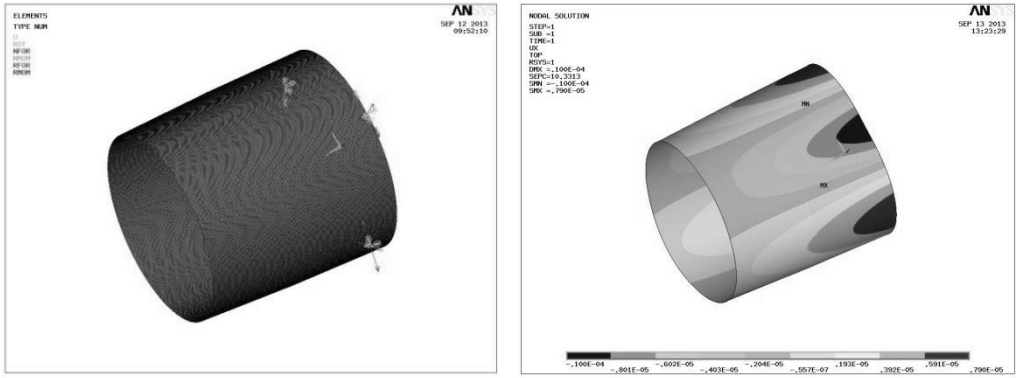

Figure 4: FEM of a mirror shell with 3 mounts at end with induced displacement of 10 μm. Loads on left; results on right.

If it were a normal-incidence optic, the raw data would be output and the optical error implied. However, for the grazing incidence optic, the raw data must be processed, leaving more room for numerical error. We are currently exploring the output of higher precision data along with utilizing the slope data output from ANSYS.

2.5.Metrology

We plan to verify the analytical and FEA models with metrology on existing test articles and new prototype configurations. We will set up test fixtures to apply forces or displacements, measure deflections and axial slope errors and then estimate performance parameters.

The metrology capabilities at MSFC are well documented in Reference 14. Some instruments are depicted in Figure 6. These include a vertical long-trace profilometer (shown), a horizontal long-trace profilometer, and a coordinate measuring machine.

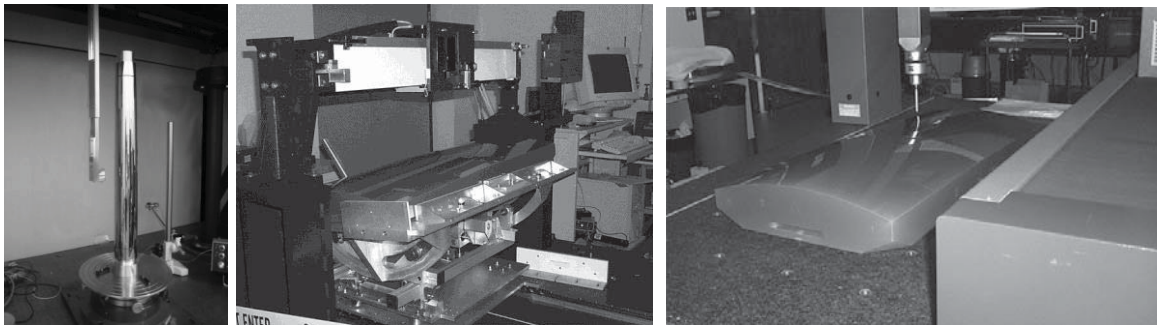

Figure 5: Photos of Vertical Long-Trace Profilometer, from Continental Optics (left), Horizontal Long-Trace Profilometer from Ocean Optics (center), and Zeiss MC850 coordinate measuring machine (right).

The Vertical Long-Trace Profilometer (VLTP, from Continental Optics) vertically scans the surface under test (SUT) (sitting on a rotary table) and is best suited for metrology of full-cylinder mirror shells and large-diameter mandrels. The Horizontal Long-Trace Profilometer (HLTP, from Ocean Optics) horizontally scans the SUT and is best suited for metrology of segment (slab) mandrels and small-diameter full-cylinder mandrels. Through interference of two closely spaced parallel pencil beams, LTPs directly measure slope deviations, which typically dominate the error budget for x-ray optics. The HLTP's accuracy has been confirmed through comparison of profile measurements of precision reference mirrors, with those obtained using a ZYGO phase-measuring interferometer (PMI). The resulting differences in profiles correspond to 0.80-μrad RMS slope-deviation accuracy. MSFC's coordinate measuring machine (CMM) is a Zeiss MC850 with a contact probe.[14]

3. INITIAL RESULTS FOR SHELLS

This section describes our initial findings for a simple full-shell mounting configuration, defined in Section 3.1. Then, Section 3.2 illustrates the parametric studies of our analytical and FEA models of the shell. Section 3.3 identifies the optimal axial location to mount the specified shell.

3.1. Configuration

Our initial configuration is a minimal concept, described in Section 2.2. The cylindrical shell is made of replicated Nickel and has the physical parameters listed in Table 1. In this concept the shell will be supported at three point-like locations. The points are azimuthally symmetric and axially coplanar. For tolerancing studies, we will displace the points radially to simulate physical tolerance uncertainties. The environment is zero-g and isothermal.

Table 1: Shell Parameters. The Young's Modulus is typical of plated Nickel alloys used in replicated optics.

Length, L	0.198 m
Radius, R	0.113 m
Thickness, τ	80 μm
Poisson's Ratio, μ	0.3
Young's Modulus, E	130 GPa

3.2.Parametric studies

Using the analytical approach, we assume a uniform deflection at one of the mounting points while holding the others fixed. With these three point constraints, the deflection pattern is determined as outlined in Section 2.4. The single point deflection results in a displacement of the axis of symmetry and a deflection pattern with three-fold symmetry. The displacement is easily removed as an azimuthal first-harmonic term, leaving only the three-fold deflections. (Note that this specific formulation holds the azimuthal angles of the mounting points constant through the deflection, and therefore neglects the slight azimuthal asymmetry introduced by the single point deflection.) The integral of the strain energy over the shell volume is equal to the work done by the deflection of the three mounting points relative to the displaced center. The work is $\sum_{i=1}^{3} k\eta_i^2 / 2$, where k is the spring constant and η_i is the deflection of the mounting point. The analytical solutions for total strain energy and spring constant as a function of axial mounting location, Z, and spring constant as a function of thickness are shown in Figure 6.

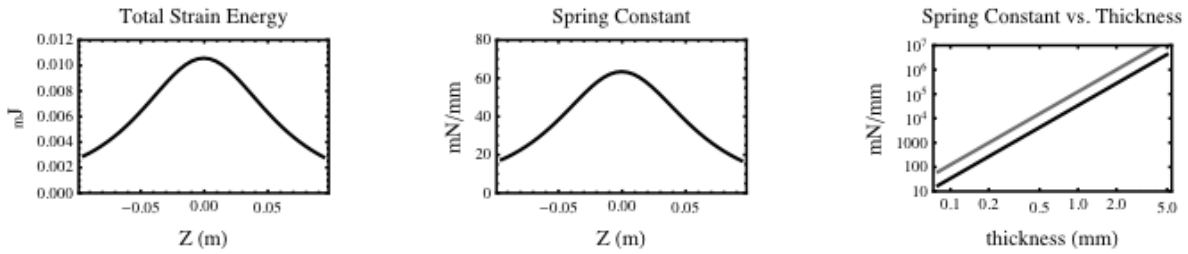

Figure 6: The left plot is the total strain energy for a 1 mm single-point deflection (mJ) vs. axial mounting location, Z. The center plot is the spring constant as a function of axial mounting location. The plot on the right shows the spring constant dependency on thickness, where the black curve is the minimum corresponding to the shell ends and the gray curve is the maximum at the shell center.

In the left plot of Figure 6, the total strain energy for a 1 mm single-point deflection indicates values of strain energy between 3 and 10 μJ. This illustrates the small amount of strain introduced in a thin shell from a relatively large deflection. Most of the deflection is linear and doesn't contribute much to the strain energy. Mainly the strain is produced from induced curvature. The center figure is a conversion to spring constant, which is proportional to the energy at a constant deflection. The plot suggests that a given amount of force will result in 3 times as large deflection if applied at the edge than if applied at the center. This suggests that flexure mounting at the center within a given tolerance would introduce less deflection, and therefore better optical performance, than flexures at the ends.

The figure on the right shows the well known fact that the spring constant varies as thickness cubed. Thus in a zero-g environment a 1 mm thick shell is 1000 times less susceptible to mounting distortion than a 100 μm shell. Since mass and size are the dominant cost drivers for space missions, this strong dependence of stiffness on thickness is the root cause of the inevitable trade between effective area and performance.

3.3.Effects of axial mounting location on performance

This section addresses the straight forward question: where is the best axial location to position the three mounting points. Given a functional form for the axial and azimuthal dependence of the axial-mean-subtracted axial slope error, $\varepsilon(Z,\theta)$, we can derive a performance figure of merit as the 2-reflection RMS angular deviation,

$$\sigma_2 = \sqrt{4/(\pi L)\int_{-L/2}^{0}\int_{0}^{2\pi}(\varepsilon(Z,\theta)-\varepsilon(L-Z,\theta))^2\,d\theta dZ}\,.$$

For Gaussian distributed errors the half-power diameter (HPD) would correspond to $1.35\times\sigma_2$, however here we have an error pattern of specific functional form so the relationship is defined by the function. Nevertheless, we find that a ratio of σ_2/HPD of 1.2-1.4 for the analytical model solutions. The plots in Figure 7 show theoretical error as a function of the axial mounting location, *Z*, where Z=0 is the axial center of the shell and $Z = L/2 = 0.099$ m is an end.

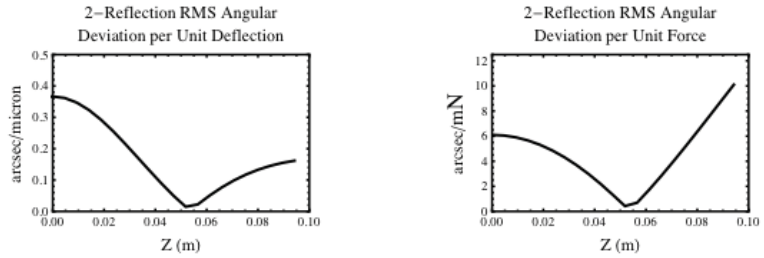

Figure 7: The plots show theoretical error as a function of the axial mounting location, Z, where Z=0 is the axial center of the shell and Z=0.099 m is an end.

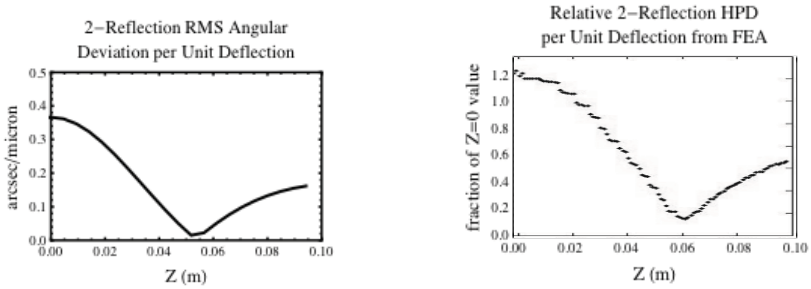

Figure 8: The analytical results are shown on the left; the FEA results on the right show the same trend.

Figures 7 and 8 show a clear minimum around 50-60% of the half-length from the center. The existence of the minimum point suggests that *there is an axial location where the performance is almost totally decoupled from mounting-point deflection*. The mounting location with the minimum error appears to be analogous to the *Airy Point.*[15] The Airy point is the support position that minimizes bending, which is located 0.577x the distance from the center.

The FEA results in Figure 8 show the same trend as the analytical data, but FEA outputs a significantly smaller error than the analytical results. Both models have the same deflection pattern as shown in Figure 7, on the left. The analytical results use only low order spatial frequency, and the

FEA some high spatial frequency deformation as well. The discrepancy could explain the difference between the models, but we will investigate further.

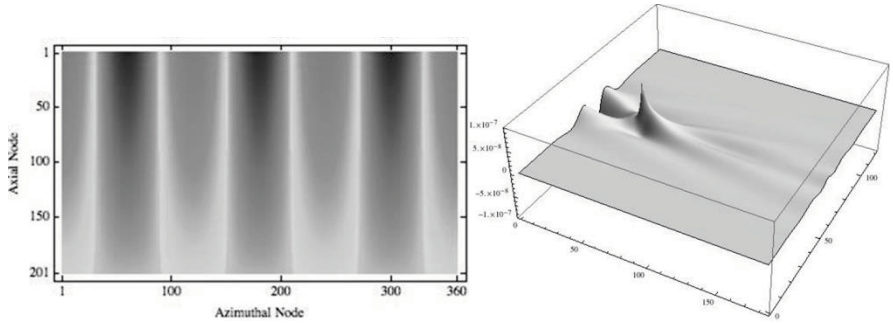

Figure 9: Resulting FEA output on left; FEA output on right after subtracting out the low spatial frequency.

Figure 10 shows the same trend in FEA, while varying the thickness of the shell.

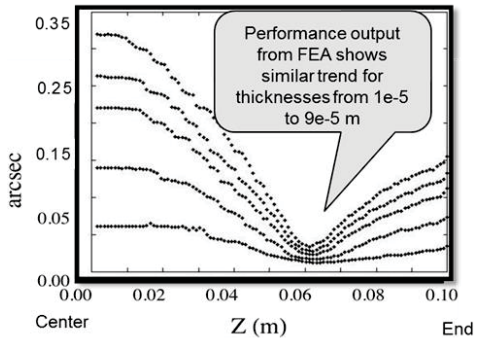

Figure 10: FEA results using shell thickness from 1e-5m through 9e-5 m.

Although still preliminary, we are confident of the existence of the performance-decoupled points. An intuitive argument for their existence is to compare the shape of the distorted shell while pushing in the center and then the shape while pushing at the end. In moving the mounting points from center to edge, the shell goes from convex to concave. It makes sense that somewhere between is a mounting location that transitions from convex to concave, minimizing the distortion.

3.4. Future plans

In the near term, further work will include validation of the results of Section 3.3 by metrology, as well as reconciling the discrepancy in performance/deflection between the two methods. It's likely that the discrepancy is the result of both the low order expansion in the analytical method and an issue with precision for the FEA data processing.

The next stage of analysis will be to add the required complexities: prescription, primary-secondary interface, bonding under a gravity load, effect of gravity on the shells during metrology, detailed mount features. Next, we will analyze segmented designs, active components, and do a parametric study of the details of the mounting structure.

We expect that the alignment precision needed for arcsecond quality optics requires an integration of flexure designs and assembly techniques into a system level process simulation rather than simply a statics model. As with the results above, we plan to begin with simple concepts which

provide adequate fidelity to identify tall poles and clear optimization paths. We will assess these concepts with a set of tools which span the entire manufacturing and integration cycle while weighing factors that affect performance and performance per unit cost. Eventually, we will construct prototypes and test articles based on the best of the vetted concepts and begin to advance our technical readiness.

3.5. Summary

Performance of x-ray optics is a complex function of many terms involving parameters of fabrication, alignment and assembly. For thin shells, sensitivity to alignment and assembly procedures increases rapidly. Although we are just at the beginning of our investigation, we have demonstrated that careful attention to design parameters can drastically reduce this sensitivity. As we gain experience in this very specialized area, we expect to discover other optimization schemes while also uncovering potential pitfalls. Through this process our goal is to shorten the development and manufacturing time for flight optics modules, while ensuring that the best performance possible is maintained.

REFERENCES

[1] Weisskopf, M.C., Aldcroft, T.L., Bautz, M., Cameron, R.A., Dewey, D., Drake, J.J, Grant, C.E., Marshall, H.L., and Murray, S.S, "An Overview of the Performance of the *Chandra X-ray Observatory*", Exp. Astron. 16, 1–68 (2003).

[2] Weisskopf, M.C., Brinkman, B., Canizares, C., Garmire, G., Murray, S., and Van Speybroeck, L.P., "An Overview of the Performance and Scientific Results from the *Chandra X-Ray Observatory*", Pub. Astron. Soc. Pac. 114, 1–24 (2002).

[3] Weisskopf, M.C., Tananbaum, H.D., Van Speybroeck, L.P., and O'Dell, S.L., "*Chandra X-ray Observatory* (CXO): overview," Proc. SPIE 4012, 2–16 (2000).

[4] Aschenbach, B., Briel, U.G., Haberl, F., Braeuninger, H. W., Burkert, W., Oppitz, A., Gondoin, P. and Lumb, D.H., "Imaging performance of the XMM-Newton x-ray telescopes," Proc. SPIE 4012, 731-739 (2000).

[5] Jansen, F., Lumb, D., Altieri, B., Clavel, J., Ehle, M., Erd, C., Gabriel, C., Guainazzi, M., Gondoin, P., Much, R., Munoz, R., Santos, M., Schartel, N., Texier, D. and Vacanti, G., "XMM-Newton observatory. I. The spacecraft and operations," Astron. and Astrophys. 365, L1-L6 (2001).

[6] Aschenbach, B., "In-orbit performance of the XMM-Newton x-ray telescopes: images and spectra," Proc. SPIE 4496, 8-22 (2002).

[7] Ramsey, B.D., Atkins, C., Gubarev, M.V., Kilaru, K., O'Dell, S.L., "Optics requirements for x-ray astronomy and developments at the Marshall Space Flight Center," Nuclear Instruments and Methods in Physics Research A 616, 110 (2012).

[8] Ramsey, B.D., Engelhaupt, D., Speegle, C., Austin, R.A., Kolodziejczak, J.J., O'Dell, S.L. and Weisskopf, M.C., "The HERO Program, High-Energy Replicated Optics for a Hard-X-Ray Balloon Payload" Proc. SPIE 3765, 816-821 (1999).

[9] Citterio, O., Citvani, M.M., Arnold, J., Campana, S., Combrinck, H., Conconi, P., Controneo, V., Freeman, R., Mattaini, E., Morton, R., Motta, G., Pareschi, G., Parodi, G., Proserpio, L., Schuler, S., Simpson, P., Tagliaferri, G. and Walker, D., "Progress on precise grinding and polishing of thin monolithic shell (towards WFXT)," Proc. SPIE 8147, 14-25 (2011).

[10] Collon, M.J., Gunther, R., Ackermann, M., Partapsing, R., Vacanti, G., Beijersbergen, M.W., Bavdaz, M., Wille, E., Wallace, K., Olde Riekerink, M., Lansdorp, B., de Vrede, L., van Baren, C. Muller, P., Krumrey, M. and Freyberg, M., "Silicon pore x-ray optics for IXO," Proc. SPIE 7732, 1F (2010).

[11] Alcock, S.G. and Cockerton, S., "A preferential coating technique for fabricating large, high quality optics," Nuclear Instruments and Methods in Physics Research A, 616, 110 (2010).

[12] P.B. Reid, T.L. Aldcroft, V. Cotroneo, W. Davis, R.L. Johnson-Wilke, S. McMuldroch, B.D. Ramsey, D.A. Schwartz, S. Trolier-McKinstry, A. Vikhlinin, H. Rudeger, R.H.T Wilke, "Technology development of adjustable grazing incidence x-ray optics for sub-arc second imaging," Proc. SPIE 8443, 29 (2012).

[13] Ventsel, E. and Krauthammer, T., [Thin Plates and Shells: Theory: Analysis, and Applications, 1st edition], CRC Press, (2001).

[14] Gubarev, M.V., O'Dell, S.L., Kester, T.J., Lehner, D.L., Jones, W.D., Smithers, M.E., Content, D.A. and Reid, P.B., "Incoming metrology of segmented x-ray mandrels at MSFC", Proc. SPIE 5494, 447–458 (2004).

[15] Phelps, F. M., "Airy Points of a Meter Bar," Amer. J. Physics 34(5), 419-422 (1966).